

On the Optimal Beamwidth of UAV-Assisted Networks Operating at Millimeter Waves

Manishika Rawat*, Marco Giordani*, Brejesh Lall†, Abdelaali Chaoub‡, and Michele Zorzi*

*Department of Information Engineering, University of Padova, Padova, Italy

†Department of Electrical Engineering, Indian Institute of Technology Delhi, New Delhi, India

‡National Institute of Posts and Telecommunications (INPT), Rabat, Morocco

E-mails: manishika.rawat8@gmail.com, giordani@dei.unipd.it, brejesh@ee.iitd.ac.in, chaoub.abdelaali@gmail.com, zorzi@dei.unipd.it

Abstract—The millimeter-wave (mm-wave) bands enable very large antenna arrays that can generate narrow beams for beamforming and spatial multiplexing. However, directionality introduces beam misalignment and leads to reduced energy efficiency. Thus, employing the narrowest possible beam in a cell may not necessarily imply maximum coverage. The objective of this work is to determine the optimal sector beamwidth for a cellular architecture served by an unmanned aerial vehicle (UAV) acting as a base station (BS). The users in a cell are assumed to be distributed according to a Poisson Point Process (PPP) with a given user density. We consider hybrid beamforming at the UAV, such that multiple concurrent beams serve all the sectors simultaneously. An optimization problem is formulated to maximize the sum rate over a given area while limiting the total power available to each sector. We observe that, for a given transmit power, the optimal sector beamwidth increases as the user density in a cell decreases, and varies based on the height of the UAV. Thus, we provide guidelines towards the optimal beamforming configurations for users in rural areas.

Index Terms—UAV-BS, millimeter-wave, optimal sector beamwidth, rural connectivity.

I. INTRODUCTION

According to the World Bank, 43 % of the world population lives in rural areas [1]. However, these regions remain mostly unserved while the world prepares to roll out the fifth generation (5G) of mobile networks. According to a report published by the International Telecommunication Union in 2021, the share of Internet users in urban areas is twice the number in rural areas [2]. The primary cause behind this is the lack of communication infrastructure in remote areas. The next generation of wireless networks (6G) emerges as a solution to this challenge [3]: for example, 6G is focusing on non-terrestrial networks (NTN) using Unmanned Aerial Vehicles (UAVs), High Altitude Platforms (HAPs), and satellites to promote ubiquitous and high-capacity global connectivity [4]. Notably, these modules can serve as aerial base stations (BS) or to assist the terrestrial BS in providing on-demand, cost-effective coverage in unserved and poorly served areas [5].

UAVs, in particular, have been proposed to bridge the digital divide and provide on-demand networks for applications such as disaster management, medical camps, network exploration, and surveillance [6], [7]. Deploying a UAV as a BS (UAV-BS)

is quick and affordable compared to a terrestrial network infrastructure, and when operating in the millimeter-wave (mm-wave) bands can promote cost-effective ubiquitous coverage, high throughput, and low latency even in rural areas [8].

However, how to deploy UAV-BSs is a challenging design issue, and has been discussed in detail in [9], [10]. At the same time, allocating the (limited) resources to the ground users is critical. Several resource allocation problems have been formalized in the literature to meet different quality of service (QoS) requirements such as coverage, fairness, and energy efficiency [11]–[17]. An energy-efficient UAV communication system was proposed in [11] by optimizing the UAV trajectory and jointly considering the communication throughput and the energy consumption. In [12], the authors introduced an approximate beam pattern and provided a solution for the UAV deployment and beam gain allocation to maximize the capacity over a given area. In [13], multi-UAV communication and non-orthogonal multiple access (NOMA) have been combined for the purpose of constructing high-capacity Internet of Things (IoT) uplink transmission systems. The channel assignment, the uplink transmit power of IoT nodes, and the flying heights of UAVs have been jointly optimized to maximize the system capacity. In [14], NOMA transmission with UAV-BS is implemented to provide coverage over a dense user region. A beam scanning approach has been proposed to identify the optimal area within the user region, and hence maximize the achievable sum rate. In [15], the locations of transceivers in the downlink and uplink were modeled using a Poisson Point Process (PPP) or Poisson Cluster Process to derive closed-form expressions of the coverage probability. In [16], an optimal resource allocation problem has been investigated for downlink coverage. It considered concurrent transmission to all sectors, and an asymptotically-optimal solution has been proposed to solve a mixed integer non-linear programming problem. The authors in [17] have proposed an intelligent UAV-BS placement and power allocation algorithm to maximize the sum rate in a region.

The optimal beamwidth for UAV-assisted multi-user systems has been studied in [18] considering the main lobe of the directional antenna serving a cell. The ground terminals were partitioned into disjoint clusters, which were sequentially served by the UAV, and the joint UAV height and beamwidth

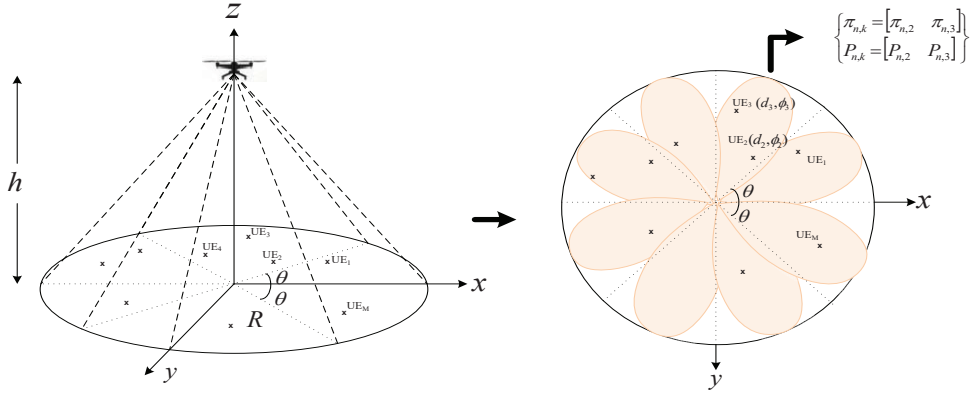


Fig. 1. Geometry of the scenario where a UAV-BS serves a cellular area of radius R .

have been investigated. The altitude, beamwidth, and location of the UAV and the bandwidth allocated to each user were jointly optimized in [19] for uplink UAV communication to minimize the sum uplink power. An algorithm was proposed to obtain a suboptimal solution by assigning different bandwidths to ground terminals. In [20], the UAV location and antenna beamwidth were jointly optimized for quasi-stationary and mobile UAVs. The impact of the beamwidth on UAV location and trajectory has been investigated for minimizing serving time and increasing throughput. All of these works, however, assume that the vertical main lobe of the UAV antenna covers all users.

In this paper we determine the optimal sector beamwidth for a UAV-assisted cellular network implementing hybrid beamforming, where users are distributed according to a PPP with a given user density. An optimization problem is developed for efficient resource allocation to maximize the sum rate in a sector while ensuring fairness. We observe that the optimal sector beamwidth depends on the user density, the height of the UAV-BS, and the propagation scenario. For a sub-urban scenario, with cell radius of 100 m and a UAV-BS deployed at a height of 100 m, the optimal beamwidth decreases from 10° to 5° as the user density increases from 0.0005 to 0.002 UEs/m². On the other hand, for a fixed user density of 0.0005 UEs/m², the optimal beamwidth initially decreases from 12° to 10° and then increases to 15° as the UAV height increases from 10 m to 200 m. We further observe that the number of sectors required to optimally serve a given number of users in an urban region is much larger than that in a rural region for the same QoS requirements.

The paper has been organized as follows. In Sec. II we present our system model; in Sec. III we describe the optimization problem to maximize the sum rate in a cell within given constraints, and present the algorithm we used to compute the sum rate as a function of the sector beamwidth; in Sec. IV we show our simulation results; conclusions are given in Sec. V.

Notations: For a random variable X , $X \sim \text{Poisson}(x)$ denotes that X is Poisson distributed with rate parameter x , $X \sim \text{U}(x_1, x_2)$ indicates that X is uniformly distributed in

the range $(x_1, x_2]$, and $X \sim \text{Tr}(x_1, x_2)$ denotes that X has triangular distribution in the range $(x_1, x_2]$ [21].

II. SYSTEM MODEL

The system model involves a UAV-BS deployed at a height h and serving a cellular area of radius R , as shown in Fig. 1. The cell is divided into S sectors, each of beamwidth θ . The UAV is mounted with a uniform planar array (UPA) antenna of N elements such that $\theta \approx 2/N$ radians [22]. The users, represented by crosses in Fig. 1, are distributed in the cell according to a PPP with density λ . The location of the k^{th} user in a cell is given by (d_k, ϕ_k) , where d_k is the horizontal distance between the k^{th} user and the UAV-BS and ϕ_k is the phase of the k^{th} user measured counterclockwise. Here, $\phi \sim \text{U}(0, 2\pi)$ and $d \sim \text{Tr}(0, R)$. The average number of users in a cell is $M = \pi R^2 \lambda$. We assume fixed transmit power P_t at the UAV, and orthogonal frequency division multiplexing (OFDM) to serve multiple users on a single beam. Therefore, the total bandwidth B is split into N_c subcarriers to serve multiple users in a sector. We operate at mm-wave frequency in an effort to maximize the communication capacity, and assume hybrid beamforming at the UAV such that all sectors are served by concurrent beams [23].

The data rate $r_{n,k}$ for the n^{th} subcarrier allocated to the k^{th} user is given by

$$r_{n,k} = (B/N_c) \log_2(1 + P_{n,k} \gamma_{n,k}), \quad (1)$$

where $\gamma_{n,k}$ is given by [24], i.e.,

$$\gamma_{n,k}(l_k) = \frac{|\mathbb{h}_{LoS}^{n,k}|^2 PL_{LoS}^{n,k}(l_k) P_r(l_k) + |\mathbb{h}_{NLoS}^{n,k}|^2 PL_{NLoS}^{n,k}(l_k) (1 - P_r(l_k))}{N_0 B / N_c G G_r}. \quad (2)$$

In Eq. (2), $l_k = \sqrt{h^2 + d_k^2}$ is the distance between the UAV and the k^{th} user, and $\mathbb{h}_{LoS}^{n,k}$ and $\mathbb{h}_{NLoS}^{n,k}$ are the path gains for the line-of-sight (LoS) and non-line-of-sight (NLoS) paths between the UAV and the k^{th} user. Specifically, $k \in \{1, 2, \dots, K_s\}$, where K_s represents the number of users in the s^{th} sector, $s \in \{1, 2, \dots, S\}$, and $n \in \{1, 2, \dots, N_c\}$. N_0

is the noise power spectral density, and G and G_r represent the beamforming gains of the transmitting and receiving antennas, respectively. $P_r(l_k)$ is the LoS probability between the UAV and the k^{th} user, and is given by

$$P_r(l_k) = \frac{1}{1 + e^{\alpha_1 \psi^3 + \alpha_2 \psi^2 + \alpha_3 \psi + \alpha_4}}, \quad (3)$$

where $\psi = \sin^{-1}(h/l_k)$ is the elevation angle of the UAV with respect to the k^{th} user, and α_1 , α_2 , α_3 , and α_4 are parameters of the LoS probability distribution defined for sub-urban, urban, dense-urban, and high-rise-urban environments in [25, Table 2]. PL_{LoS} and PL_{NLoS} represent the path losses for LoS and NLoS links; for mm-wave communication [26], they are expressed in dB as

$$PL_{LoS}(l_k) = 61.4 + 20 \log_{10}(l_k) + \mathcal{N}(0, 33.64); \quad (4)$$

$$PL_{NLoS}(l_k) = 72.0 + 29.2 \log_{10}(l_k) + \mathcal{N}(0, 75.69). \quad (5)$$

where, $\mathcal{N}(\mu, \sigma^2)$ represents a normal random variable with mean μ and variance σ^2 . In the following section we will develop an optimization problem to maximize the sum rate in a cell while limiting the total power available in a sector.

III. SUM RATE MAXIMIZATION PROBLEM

The sum rate maximization problem for a sector can be expressed as:

$$\max_{\pi_{n,k}, P_{n,k}} \sum_{k=1}^{K_s} \sum_{n=1}^{N_c} r_{n,k} \pi_{n,k} \quad (6a)$$

$$\text{s.t.} \quad C_1 : \sum_{k=1}^{K_s} \pi_{n,k} \leq 1 \quad \forall n, \quad (6b)$$

$$C_2 : \sum_{n=1}^{N_c} r_{n,k} \pi_{n,k} \geq R_0 \quad \forall k, \quad (6c)$$

$$C_3 : \sum_{k=1}^{K_s} \sum_{n=1}^{N_c} P_{n,k} \leq \frac{P_t \theta}{360}, \quad (6d)$$

$$C_4 : \pi_{n,k} \in \{0, 1\} \quad \forall n, k, \quad (6e)$$

$$C_5 : P_{n,k} \geq 0 \quad \forall n, k. \quad (6f)$$

In (6a), we introduce a binary variable $\pi_{n,k}$ to ensure that at least one subcarrier is allocated to one user in a sector in the beam serving time. Here, θ is the beamwidth of a sector, and R_0 is the bit rate. $P_{n,k}$ is the power transmitted over the n^{th} subcarrier allocated to the k^{th} user. Constraints C_1 and C_4 ensure that the same subcarrier is not allocated to different users, and thus $\pi_{n,k}$ can take only binary values such that the sum across the users is less than or equal to 1. C_2 ensures a minimum data rate to each user. As the cell is divided into sectors, the total power available to a sector would be proportional to the sector beamwidth. Therefore, C_3 limits the total power available to a sector. This limits the maximum data rate available to users as the sector beamwidth decreases or the number of sectors in a cell increases. C_5 ensures that the power allocated to each user is non-negative.

Algorithm 1: To compute the sum rate per cell as a function of θ for a given value of λ

```

initialize  $N_c, P_t, B, R_0, G_0, G_r, N_0, R, h, \lambda,$ 
 $\theta \in \text{div}(360),$ 
for each value of  $\theta$  do
   $S = 360/\theta;$  /*number of sectors
  for  $\eta = 1, 2, \dots, \mathbb{N};$  /*MC simulations
  do
     $\chi \sim \text{Poisson}(\pi R^2 \lambda), \phi \sim U(0, 2\pi),$ 
     $d \sim \text{Tr}(0, R);$  /*user distribution
    parameters
    for  $s = 1, 2, \dots, S$  do
      Based on the value of  $\phi_k$  and  $\theta$ , determine
      the users that lie in the  $s^{th}$  sector;
      Compute  $g_{n,k}(N_c, K_s)$  for each sector;
      Run optimization module given in (7) to
      allocate  $N_c$  subcarriers to  $K_s$  users;
      Compute  $r_{n,k}(N_c, K_s)$  for each sector;
       $Op_s(s) = \sum_{n=1}^{N_c} \sum_{k=1}^{K_s} r_{n,k}(N_c, K_s);$ 
      /*sum rate per sector
    end
     $Op_\eta(\eta) = \sum_{s=1}^S Op_s$ 
     $Ap_\eta(\eta) = Op_\eta(\eta)/\chi$ 
  end
   $Op = \sum_{\eta=1}^{\mathbb{N}} Op_\eta/\mathbb{N};$  /*sum rate per cell
   $Ap = \sum_{\eta=1}^{\mathbb{N}} Ap_\eta/\mathbb{N};$  /*average rate
end

```

The optimization problem in (6a) is a mixed integer non-linear programming problem (MINLP). Due to the non-convexity, the global optimal solution cannot be achieved. The time taken to run this module increases proportionally with the number of users and sectors. However, we can simplify the problem using the mixed integer (MI) property of $\pi_{n,k}$. The simplified optimization problem can be expressed as

$$\max_{\pi_{n,k}, P_{n,k}} \sum_{k=1}^{K_s} \sum_{n=1}^{N_c} r_{n,k} \quad (7a)$$

$$\text{s.t.} \quad C_1, C_4, C_5,$$

$$C_6 : \sum_{n=1}^{N_c} r_{n,k} \geq R_0 \quad \forall k, \quad (7b)$$

$$C_7 : \sum_{k=1}^{K_s} \sum_{n=1}^{N_c} P_{n,k} \leq \pi_{n,k} \frac{P_t \theta}{360}, \quad (7c)$$

$$C_8 : r_{n,k} \leq \pi_{n,k} R_{max} \quad \forall n, k. \quad (7d)$$

We have omitted $\pi_{n,k}$ from (7a) and (7b) to reduce the redundancy in problem formulation. The condition that $r_{n,k} = 0$ when $\pi_{n,k} = 0$ is enforced by C_8 . C_5 and C_7 ensure that $P_{n,k}$ drops to zero when $\pi_{n,k} = 0$. Thus, the algorithm needs to run only for non-zero entries in $\pi_{n,k}$, which reduces the problem complexity. R_{max} in C_8 is the maximum data rate

that can be achieved. It can be used to limit the number of iterations of the solver to save the processing time.

The resource allocation problem in (7) can be explained by taking the example of Fig. 1. Here, $S = 8$ and we set $N_c = 4$ so that both $\pi_{n,k}$ and $P_{n,k}$ for the second sector measured counterclockwise in Fig. 1 are of size 4×2 . Thus, the four subcarriers in a sector can be allocated to two users. Because of C_1 , one of the possible solutions would be

$$\pi_{n,k} = \begin{pmatrix} 1 & 0 \\ 0 & 1 \\ 0 & 1 \\ 0 & 1 \end{pmatrix}. \text{ Accordingly, } P_{n,k} = \begin{pmatrix} P_{1,2} & 0 \\ 0 & P_{2,3} \\ 0 & P_{3,3} \\ 0 & P_{4,3} \end{pmatrix} \text{ such}$$

that $\sum_{n=1}^4 \sum_{k=2}^3 P_{n,k} \leq P_t/8$.

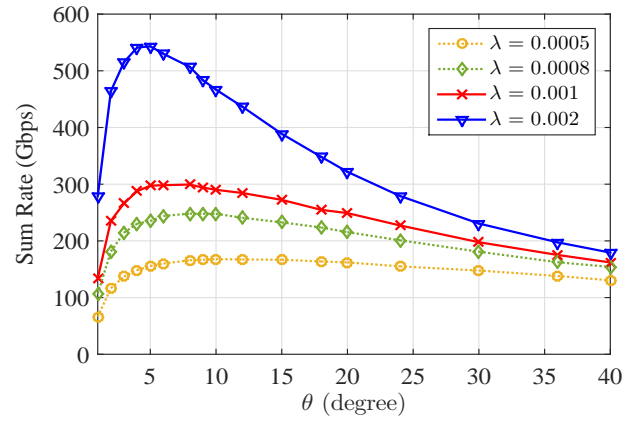
Algorithm 1 specifies the steps to compute the sum rate per cell and average rate per user as a function of θ for a given user density. First, we generate users distributed as a PPP in a cell of radius R for a given value of θ and λ . The users in the same sector are then categorized for analysis. The optimization function maximizes the sum rate per sector, which is added to produce the sum rate per cell. The average rate per user is computed by dividing the sum rate per cell by the number of users. Here, \mathbb{N} represents the number of Monte Carlo (MC) simulations and $\text{div}(x)$ represents the divisors of x .

IV. RESULTS AND DISCUSSIONS

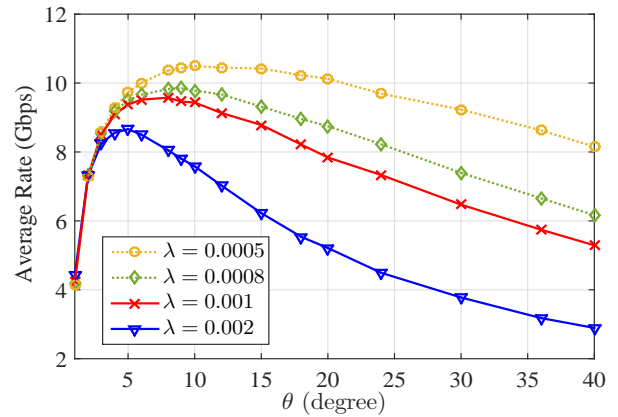
In this section, we evaluate the impact of user density and UAV height on the optimal sector beamwidth of a cell. We work with $B = 1$ GHz, $P_t = 10$ W, $N_c = 30$, $R_0 = 1$ Gbps, $R_{max} = 50$ Gbps, $f_c = 28$ GHz, and $N_0 = -174$ dBm/Hz. The channel is assumed to be Rician with a distribution parameter of 8 dB [27]. We use the solving constraint integer program (*scip*) in the General Algebraic Modeling System (GAMS), a high-level modeling system for mathematical optimization to solve the MINLP problem in (6a). We consider (i) a rural/sub-urban scenario with a lower user density $\lambda = \{0.0005, 0.0008, 0.001, 0.002\}$ UEs/m² in a cell of radius $R = 100$ m (Sec. IV-A), and (ii) an urban scenario with a higher user density $\lambda = \{0.05, 0.08, 0.1\}$ UEs/m² in a cell of radius $R = 10$ m (Sec. IV-B). The impact of the UAV height is explored in Sec. IV-C. We assume $G = N$ and $G_r = 1$ for the analysis [22]. The results have been obtained for 500 MC simulations.

A. Rural/Sub-Urban Scenario

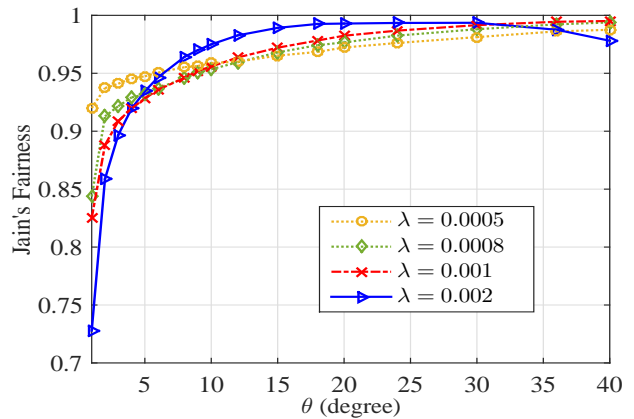
Fig. 2(a) plots the sum rate obtained by solving the optimization problem in (7) as a function of θ . The result is obtained for $R = 100$ m, $h = 100$ m, and different values of λ . First, we observe that as the user density increases, the number of users in the cell increases, thus increasing the sum rate per cell, which validates the accuracy of our results. Initially, as θ increases the sum rate also increases given that the power allocated to each sector increases proportionally. However, after a certain value of θ , the sum rate decreases exponentially. This can be attributed to the lower spatial reuse as θ increases, i.e., as the number of sectors decreases. Therefore, we conclude that the smallest beamwidth does



(a) Sum rate per cell.



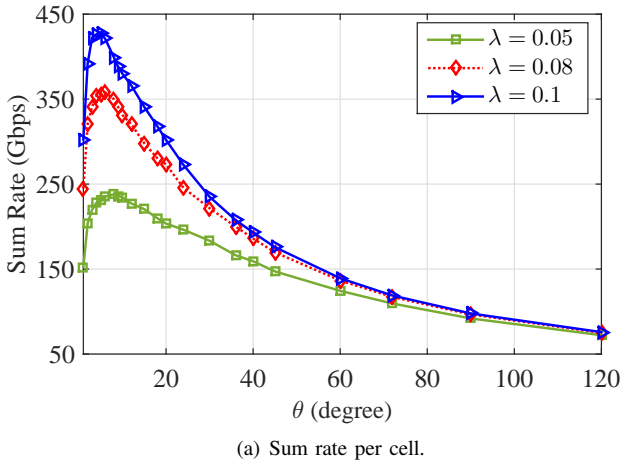
(b) Average rate per user.



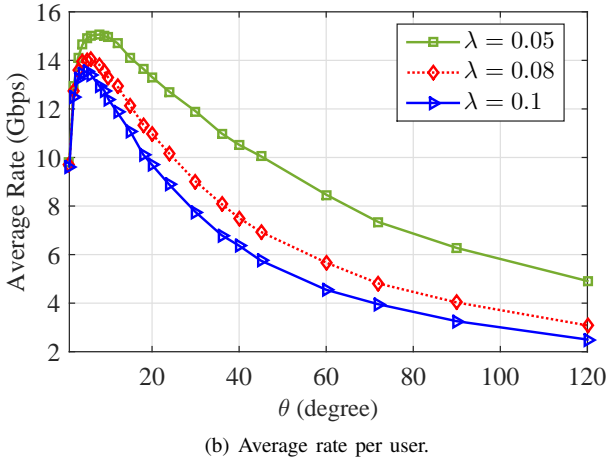
(c) Jain's fairness index.

Fig. 2. Sum rate per cell, average rate per user, and Jain's fairness index in a rural/sub-urban scenario with $R = 100$ m and $h = 100$ m, as a function of θ , for different user densities.

not necessarily ensure the maximum sum rate. The sector beamwidth at which the sum rate is maximized is represented by θ_{opt} . According to Fig. 2(a), $\theta_{opt} = 10^\circ$ for $\lambda = 0.0005$. As λ increases from 0.0008 to 0.002, θ_{opt} decreases from 9° to 5° , respectively. This implies that in a rural environment, it



(a) Sum rate per cell.



(b) Average rate per user.

Fig. 3. Sum rate per cell and average rate per user in an urban scenario with $R = 10$ m and $h = 20$ m as a function of θ , for different user densities.

is desirable to operate through wider beams as the density of users decreases.

Fig. 2(b) plots the average rate per user as a function of θ for different values of λ . The use of the mm-wave technology ensures that the rate is always above 1 Gbps, and in line with the requirements of most 5G/6G applications. As expected, as the number of users in the cell increases, the average rate per user decreases. Moreover, as θ increases the average rate also increases, and follows the same trend of the sum rate as explained in the previous paragraph. However, θ_{opt} decreases as the user density increases. This is because, as the number of users in each sector grows, the amount of power allocated to each user decreases. Consequently, in order to maximize the sum rate, the objective function drives θ towards smaller values. Therefore, we conclude that for a densely populated rural region, a higher number of sectors would be optimal.

In order to demonstrate the impact of the fairness among the users in a cell, Fig. 2(c) plots Jain's Fairness index as a function of θ for different user densities. It is computed as $J = \frac{(\sum_i R_i)^2}{M \sum_i R_i^2}$, where R_i represents

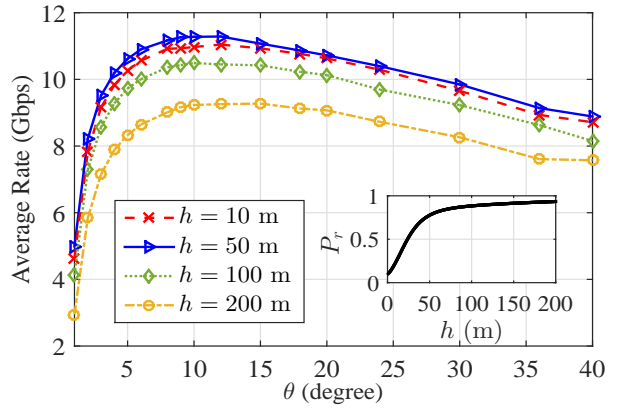


Fig. 4. Average rate per user vs. h and θ with $R = 100$ m and $\lambda = 0.0005$.

the rate per user [28]. The value of Jain's fairness index for $\lambda = \{0.0005, 0.0008, 0.001, 0.002\}$ at θ_{opt} is $\{0.96, 0.9504, 0.9461, 0.9345\}$, respectively. We observe that J increases with θ , and good fairness is achieved at the optimal sector beamwidth. This can be attributed to constraint C_6 in (7), where a minimum data rate is guaranteed to each user. Thus, we conclude that the proposed resource allocation ensures fairness among all the users in a cell.

B. Urban Scenario

Fig. 3(a) plots the sum rate as a function of θ for various user densities in a cell of radius $R = 10$ m. The UAV is deployed at $h = 20$ m. As observed in Sec. IV-A, the sum rate initially increases and then decreases exponentially after θ reaches its optimal value. However, θ_{opt} obtained here is generally smaller than in the rural/sub-urban scenario. At $\lambda = 0.05$, $\theta_{opt} = 8^\circ$ which gives $M = 15.7$ and $S = 45$ to serve the users optimally. As the user density increases from $\lambda = 0.08$ to 0.1 , θ_{opt} decreases from 6° to 5° . This implies that the number of sectors required to serve all the users increase from $S = 60$ to $S = 72$, respectively. A similar trend for the value of θ_{opt} is observed in the plot of the average rate per user in Fig. 3(b). Notice that these results were obtained up to a beamwidth of 120° , with the cell having only three sectors to provide a more comprehensive picture.

C. Impact of the UAV Height

Fig. 4 plots the average rate per user as a function of θ and h in a rural/sub-urban cell with radius $R = 100$ m and $\lambda = 0.0005$ UEs/m². The LoS probability (P_r) as a function of h defined in Eq. (3) is shown in the inset. We observe that P_r is small for $h \leq 50$ m. As a result, the average rate per user for $h = 50$ m is higher than for $h = 10$ m. As h continues to increase, the LoS probability increases, but so does the path loss. The impact of the path loss becomes the dominant factor when $h > 100$ m, even though the LoS probability also increases. The effect is also visible in the value of θ_{opt} , which decreases initially from 12° to 10° as h increases from 50 m to 100 m, and then increases to $\theta_{opt} = 15^\circ$ at $h = 200$ m. This

is because, for $50 \leq h \leq 100$ m, the path loss is relatively small, thus the optimization problem drives θ to a smaller value to increase the antenna gain and the sum rate. However, to compensate for the very high path loss at $h > 100$ m, the optimization problem attempts to increase the power allocated to the users by increasing θ_{opt} . Therefore, we conclude that the optimal sector beamwidth is a function of h .

In order to compare the optimal number of sectors required to serve a given number of users in the rural/sub-urban and urban scenarios, we consider two configurations with the same LoS probability, i.e., $R = 100$ m and $h = 50$ m, and $R = 10$ m and $h = 20$ m, respectively. For the first configuration with $\lambda = 0.0005$ and $M = 15.7$, the optimal number of sectors at θ_{opt} is $S = 30$. This is much lower than $S = 45$ obtained in the second configuration with the same number of users in Sec. IV-B. Consequently, the number of elements required in a UPA antenna decreases from $N = 15$ in an urban environment to around $N = 12$ in a sub-urban scenario. This implies a considerable reduction in the cost and complexity of the antenna system for serving a rural/sub-urban area.

V. CONCLUSION

In this work, we investigated the optimal sector beamwidth for a cell served by a UAV acting as a BS. Assuming that users are distributed according to a PPP, we observed that there is an optimal beamwidth to maximize the sum rate over a region. For a given transmit power, this optimal beamwidth is a function of the user density and the height of the UAV. Based on simulations we observed that, for the same LoS probability, $S = 45$ sectors are required in an urban region vs. $S = 30$ sectors in a rural region to optimally serve an average number of 15.7 users in a cell with the same QoS requirements. Also, we showed that a remote area with lower density of users can be optimally served by a UAV-BS flying at lower altitude. This implies lower complexity in terms of antenna size and transmit power, and less spatial reuse and interference among the sectors, respectively, compared to the urban environment. Our conclusions encourage the use of UAV-BSs to connect remote and poorly served areas.

REFERENCES

- [1] The World Bank, "Percentage of rural population," Accessed: 09/20/2022. [Online]. Available: <https://data.worldbank.org/indicator/SP.RUR.TOTL.ZS>
- [2] ITU, "Measuring digital development: Facts and figures," *Technical Report*, 2021, Accessed: 09/20/2022. [Online]. Available: <https://www.itu.int/en/ITU-D/Statistics/Pages/facts/>
- [3] M. Giordani, M. Polese, M. Mezzavilla, S. Rangan, and M. Zorzi, "Toward 6G networks: Use cases and technologies," *IEEE Commun. Mag.*, vol. 58, no. 3, pp. 55–61, Mar. 2020.
- [4] M. Giordani and M. Zorzi, "Non-terrestrial networks in the 6G era: Challenges and opportunities," *IEEE Network*, vol. 35, no. 2, pp. 244–251, Dec. 2020.
- [5] A. Chaoub, M. Giordani, B. Lall, V. Bhatia, A. Kliks, L. Mendes, K. Rabie, H. Saarnisaari, A. Singhal, N. Zhang *et al.*, "6G for bridging the digital divide: Wireless connectivity to remote areas," *IEEE Wireless Commun.*, vol. 29, no. 1, pp. 160–168, July 2021.
- [6] D. Wang, M. Giordani, M.-S. Alouini, and M. Zorzi, "The potential of multi-layered hierarchical non-terrestrial networks for 6G," *IEEE Veh. Technol. Mag.*, vol. 16, no. 3, pp. 99–107, July 2020.
- [7] A. U. Rahman, F. Fourati, K.-H. Ngo, A. Jindal, and M.-S. Alouini, "Network graph generation through adaptive clustering and infection dynamics: A step toward global connectivity," *IEEE Commun. Lett.*, vol. 26, no. 4, pp. 783–787, Jan. 2022.
- [8] M. Matracia, M. A. Kishk, and M.-S. Alouini, "Coverage analysis for UAV-assisted cellular networks in rural areas," *IEEE Open J. Veh. Technol.*, vol. 2, pp. 194–206, Apr. 2021.
- [9] I. A. Elnabty, Y. Fahmy, and M. Kafafy, "A survey on UAV placement optimization for UAV-assisted communication in 5G and beyond networks," *Phys. Commun.*, vol. 51, p. 101564, Apr. 2022.
- [10] M. Alzenad, A. El-Keyi, and H. Yanikomeroglu, "3D placement of an unmanned aerial vehicle base station for maximum coverage of users with different QoS requirements," *IEEE Wireless Commun. Lett.*, vol. 7, no. 1, pp. 38–41, Sept. 2017.
- [11] Y. Zeng and R. Zhang, "Energy-efficient UAV communication with trajectory optimization," *IEEE Trans. Wireless Commun.*, vol. 16, no. 6, pp. 3747–3760, Mar. 2017.
- [12] Z. Xiao, H. Dong, L. Bai, D. O. Wu, and X.-G. Xia, "Unmanned aerial vehicle base station (UAV-BS) deployment with millimeter-wave beamforming," *IEEE Internet of Things J.*, vol. 7, no. 2, pp. 1336–1349, Nov. 2019.
- [13] R. Duan, J. Wang, C. Jiang, H. Yao, Y. Ren, and Y. Qian, "Resource allocation for multi-UAV aided IoT NOMA uplink transmission systems," *IEEE Internet of Things J.*, vol. 6, no. 4, pp. 7025–7037, Apr. 2019.
- [14] N. Rupasinghe, Y. Yapıcı, I. Güvenç, and Y. Kakishima, "Non-orthogonal multiple access for mm-wave drone networks with limited feedback," *IEEE Trans. Commun.*, vol. 67, no. 1, pp. 762–777, Aug. 2018.
- [15] W. Yi, Y. Liu, E. Bodanese, A. Nallanathan, and G. K. Karagiannidis, "A unified spatial framework for UAV-aided mmwave networks," *IEEE Trans. Commun.*, vol. 67, no. 12, pp. 8801–8817, Oct. 2019.
- [16] S. Kumar, S. Suman, and S. De, "Dynamic resource allocation in UAV-enabled mmwave communication networks," *IEEE Internet Things J.*, vol. 8, no. 12, pp. 9920–9933, Sept. 2021.
- [17] Z. Kaleem, W. Khalid, A. Muqabel, A. A. Nasir, C. Yuen, and G. K. Karagiannidis, "Learning-aided UAV 3D placement and power allocation for sum-capacity enhancement under varying altitudes," *IEEE Commun. Lett.*, vol. 26, no. 7, pp. 1633–1637, May 2022.
- [18] H. He, S. Zhang, Y. Zeng, and R. Zhang, "Joint altitude and beamwidth optimization for UAV-enabled multiuser communications," *IEEE Commun. Lett.*, vol. 22, no. 2, pp. 344–347, Feb. 2018.
- [19] Z. Yang, C. Pan, M. Shikh-Bahaei, W. Xu, M. Chen, M. El-kashlan, and A. Nallanathan, "Joint altitude, beamwidth, location, and bandwidth optimization for UAV-enabled communications," *IEEE Commun. Lett.*, vol. 22, no. 8, pp. 1716–1719, Aug. 2018.
- [20] N. Tang, H. Tang, B. Li, and X. Yuan, "Joint maneuver and beamwidth optimization for UAV-enabled multicasting," *IEEE Access*, vol. 7, pp. 149 503–149 514, Oct. 2019.
- [21] M. Rawat, B. Lall, and S. Srirangarajan, "Statistical characterization of the angle of arrival in an underwater channel due to scattering from the sea surface modeled as sum of sinusoids," *IEEE Trans. Veh. Technol.*, vol. 71, no. 2, pp. 1562–1574, Nov. 2021.
- [22] C. A. Balanis, *Antenna Theory: Analysis and Design*, 4th ed. John Wiley & Sons, Inc, 2015.
- [23] Y. Wang, M. Giordani, X. Wen, and M. Zorzi, "On the beamforming design of millimeter wave UAV networks: Power vs. capacity trade-offs," *Computer Networks*, vol. 205, p. 108746, Mar. 2022.
- [24] N. Varshney and S. De, "Optimum downlink beamwidth estimation in mm-wave communications," *IEEE Trans. Commun.*, vol. 69, no. 1, pp. 544–557, Sept. 2020.
- [25] I. Mohammed, I. B. Collings, and S. V. Hanly, "Line of sight probability prediction for UAV communication," in *IEEE ICC Workshops, Montreal, QC, Canada*, June 2021, pp. 1–5.
- [26] M. R. Akdeniz, Y. Liu, M. K. Samimi, S. Sun, S. Rangan, T. S. Rappaport, and E. Erkip, "Millimeter wave channel modeling and cellular capacity evaluation," *IEEE J. Sel. Areas Commun.*, vol. 32, no. 6, pp. 1164–1179, June 2014.
- [27] T. Zhou, C. Tao, L. Liu, and Z. Tan, "Ricean k-factor measurements and analysis for wideband radio channels in high-speed railway u-shape cutting scenarios," in *Proc. 79th IEEE Veh. Technol. Conf. (VTC Spring), Seoul, South Korea*, May 2014, pp. 1–5.
- [28] J. V. Evangelista, Z. Sattar, G. Kaddoum, and A. Chaaban, "Fairness and sum-rate maximization via joint subcarrier and power allocation in

uplink SCMA transmission," *IEEE Trans. Wireless Commun.*, vol. 18, no. 12, pp. 5855–5867, Sept. 2019.